***Jñānābha*, Vol. 50(2) (2020), 254-264**
(Dedicated to Honor Dr. R. C. Singh Chandel on His 75^{th} Birth Anniversary Celebrations)

SLIP FLOW AND HEAT TRANSFER OF MHD POWER LAW FLUID OVER A POROUS SHEET IN THE PRESENCE OF JOULE HEATING AND HEAT SOURCE/SINK

By
Sushila Choudhary and Bhagawan Singh Yadav
Department of Mathematics, University of Rajasthan, Jaipur-302004, Rajasthan, India
Email:sumathru11@gmail.com, bhagawansingh4030@gmail.com
(*Received : October* 08, 2020 *; Revised: December* 11, 2020)
DOI: https://doi.org/10.58250/jnanabha.2020.50230

Abstract

An analysis has been carried out to study the *MHD* flow and heat transfer of a non-Newtonian power-law fluid over a porous sheet in the presence of partial slip and Joule heating. Here, thermal conductivity is assumed as a function of temperature. An external heat source is also applied. The governing equations are reduced into the system of non-linear ordinary differential equations by using similarity transformations. This system along with appropriate boundary conditions are solved numerically using the shooting technique with Runge-Kutta fourth order iteration scheme. The effects of suction/injection parameter, Eckert number and heat source parameter on the velocity and temperature profiles are studied. It is observed that the temperature profile increases with decreasing value of heat source parameter, Eckert number and suction/injection parameter. The influence of different parameters on the velocity and temperature profile is presented through graphs. The effect of all physical parameters on skin friction and local Nusselt number is displayed through tables.
2010 Mathematics Subject Classifications: 76A05, 76S05, 76W05, 65L06.
Keywords and phrases: Power law fluid, joule heating effects, MHD, porous sheet, porous medium, partial slip, heat source/sink, thermal radiation.

1 Introduction

The power-law fluids are used in a wide range of industrial applications. The power-law model is useful from chemical and petrochemical processes to food industries and biotechnology. Some examples include blood flow simulation, polymer solutions, bio colloids, etc. The power-law model is one of the models which has been used by researchers for simulating the non-Newtonian fluids. One reason for this popularity is the ability to simulate a wide range of non-Newtonian fluids by this model. In the pioneering work of Schowalter [21], the applicability of boundary layer theory to the two and three-dimensional flow of pseudoplastic power-law fluids was provided. In his work, particular emphasis has been given to the formulation of boundary-layer equations which provide similar solutions. Sarpkaya [19] carried out a study on the flow of non-Newtonian fluids under the effect of a magnetic field. Sarpkaya studied the laminar flow of Bingham plastics and dilatant substances between two parallel planes under the influence of a constant pressure gradient and a steady magnetic field perpendicular to the direction of motion. Throughout this study the generalized magnetic Reynolds number has been assumed to be sufficiently small. Non-Newtonian flow through porous media has been described by Savins [20]. Gupta and Gupta [13] investigated heat and mass transfer on a stretching sheet with suction or blowing. Numerical solution of the laminar boundary layer equation for power-law fluids was described by Andersson and Toften [3]. Alberta et al. [8] investigated some similarity solutions to shear flows of non-Newtonian power-law fluids. They described the flow resistance to the vertical motion of a slender circular body in an unbounded power law fluid, which constitutes a Stokes' first problem for a circular rod. Sharma and Mathur [18] have analyzed steady laminar free convection flow of an electrically conducting fluid along a porous hot vertical plate in the presence of heat source/sink. MHD flow of a power-law fluid over a rotating disk was discussed by Andersson and Korte [4]. Andersson et al. [5] carried out a study on slip flow past a stretching surface. Free convection flow with thermal radiation and mass transfer past a moving vertical porous plate has been investigated by Makinde [16]. Yurusoy [22] considered unsteady boundary layer flow of power-law fluid on stretching sheet surface. Effects of magnetic field and suction/injection on convection heat transfer of non-Newtonian power-law fluids past a power-law stretched sheet with surface heat flux was investigated by Chen [10]. Abel et al. [2] has analysed flow and heat transfer in a power-law fluid over a stretching sheet with variable thermal conductivity and non-uniform heat source. Mahmoud [15] studied slip velocity effect on a non-Newtonian power-law fluid over a moving permeable surface with heat generation. Mukhopadhyay [17] presented heat transfer analysis of the unsteady flow of a Maxwell fluid over a stretching surface in the presence of a heat source/sink. Abdel-Rahman [1] analyzed effect of variable viscosity and thermal conductivity on unsteady MHD flow of non-Newtonian fluid over a stretching porous sheet. Steady boundary layer slip flow along with heat and mass transfer over a flat porous plate embedded in a porous medium was discussed by Aziz et al. [7]. Heat transfer analysis for stationary boundary layer slip flow of a power-law fluid in a Darcy porous medium with plate suction/injection was done by Aziz et al. [6]. In their studies, they extended the work to steady boundary layer slip flow and heat transfer over a flat plate embedded in a porous media and investigated the slip effect on boundary layer flow of a power-law fluid including heat transfer over a porous flat sheet embedded in a porous medium. Kiyasatfar and Pourmahmoud [14] considered laminar *MHD* flow and heat transfer of power-law fluids in square micro channels.

The present study focuses on the Joule heating effect with non-Newtonian power law fluid over a porous sheet in the presence of heat source/sink. The governing system of partial differential equations has been adapted using appropriate similarity transformation to nonlinear ordinary differential equations which are then solved using fourth-order Runge kutta method with the shooting technique. The effect of various physical parameters on the dimensionless velocity and temperature profiles are plotted and discussed in the result section.

2 Mathematical Formulation

Consider the steady *2-D* laminar flow of an incompressible power-law fluid under the influence of magnetic field and thermal radiation, over a semi-infinite porous sheet in a porous medium. The applied magnetic field (B) is acting normal to the sheet and induced magnetic field is considered negligible as compared to applied magnetic field, because the Reynolds number for the flow is taken to be small. The surface of the sheet is insulated and admits partial slip condition. The origin of the coordinates is at the leading edge of the sheet, the x-axis along with the sheet and y-axis normal to it. The temperature of the sheet is T_w. The velocity and temperature far away from the sheet are U_∞ and T_∞, respectively. Using boundary layer approximation the governing equations for the problem along with the slip boundary conditions are as follows

$$\frac{\partial u}{\partial x} + \frac{\partial v}{\partial y} = 0, \tag{2.1}$$

$$u\frac{\partial u}{\partial x} + v\frac{\partial u}{\partial y} = \frac{1}{\rho}\frac{\partial \tau_{xy}}{\partial y} - \frac{1}{\rho A}(u - U_\infty) - \frac{\sigma B^2}{\rho}(u - U_\infty), \tag{2.2}$$

$$u\frac{\partial T}{\partial x} + v\frac{\partial T}{\partial y} = \frac{1}{\rho C_p}\left\{\frac{\partial}{\partial y}\left[\kappa(T)\frac{\partial T}{\partial y}\right] - \frac{\partial q_r}{\partial y}\right\} + \frac{\sigma B^2}{\rho C_p}u^2 + \frac{Q}{\rho C_p}(T - T_\infty), \tag{2.3}$$

$$\begin{cases} u = L_1\frac{\partial u}{\partial y}, v = v_w, T = T_w + D_1\frac{\partial T}{\partial y}, \text{ at } y = 0, \\ u \to U_\infty, T \to T_\infty \text{ as } y \to \infty, \end{cases} \tag{2.4}$$

where u and v are the velocity components in x and y directions, ρ is the fluid density, τ_{xy} is the shear stress tensor, A is the permeability, σ is the electrical conductivity, B is the applied magnetic field, T is the temperature, C_p is the specific heat, κ is the variable thermal conductivity, q_r is the radiative heat flux, L_1 is the velocity slip factor, D_1 is the thermal slip factor, Q is the heat source parameter and v_w describes suction/blowing through the porous sheet.

The shear stress component τ_{xy} for the power-law fluid model, as derived by Bird et al. [9] is

$$\tau_{xy} = K|\frac{\partial u}{\partial y}|^{n-1}\frac{\partial u}{\partial y}, \tag{2.5}$$

where K is the consistency coefficient and n is the power-law index. In equation (5) $n = 1$ represents the Newtonian behaviour of the fluid. In the case of $n < 1$ behaviour of the fluid is known as shear-thinning, which is categorized by an apparent viscosity which decreases with increase in shear rate. In the case of $n > 1$ fluid behaviour is called shear-thickening and characterized by an apparent viscosity which increases with an increase in shear rate Chhabra et al. [11]. Therefore, a single parameter n describes the nature of fluid behaviour. Substitution of equation (2.5) in equation (2.2) gives

$$u\frac{\partial u}{\partial x} + v\frac{\partial u}{\partial y} = \frac{1}{\rho}\frac{\partial}{\partial y}\left(K\left|\frac{\partial u}{\partial y}\right|^{n-1}\frac{\partial u}{\partial y}\right) - \frac{1}{\rho A}(u - U_\infty) - \frac{\sigma B^2}{\rho}(u - U_\infty). \tag{2.6}$$

Following Das [12], we consider the temperature dependent thermal conductivity and radiative heat flux of the form

$$\kappa_T = \kappa_\infty\left(1 + \epsilon\frac{T - T_\infty}{\Delta T}\right), q_r = -\frac{16T_\infty^3\sigma}{3k}\frac{\partial T}{\partial y}, \tag{2.7}$$

where ϵ is the thermal conductivity parameter, κ_∞ is the thermal conductivity at ambient temperature and $\Delta T = T_w - T_\infty$, σ is the Stefan-Boltzmann constant and k is the mean absorption coefficient. Substitution of equation (2.7) into equation (2.3) gives

$$u\frac{\partial T}{\partial x} + v\frac{\partial T}{\partial y} = \frac{1}{\rho C_p}\left\{\frac{\partial}{\partial y}\left[k_\infty\left(1 + \epsilon\frac{T - T_\infty}{\Delta T}\right)\frac{\partial T}{\partial y}\right] + \frac{16T_\infty^3\sigma}{3k}\frac{\partial^2 T}{\partial y^2}\right\} + \frac{\sigma B^2}{\rho C_p}u^2 + \frac{Q}{\rho C_p}(T - T_\infty). \tag{2.8}$$

3 Method of solution

Now we will transform the system of equations (2.1), (2.6) and (2.8) along with the boundary conditions (2.4) into a dimensionless form. For this purpose, we choose a stream function $\Psi(x, y)$ such that

$$(3.1)\quad u = \frac{\partial \Psi}{\partial y}, v = -\frac{\partial \Psi}{\partial x}.$$

Equation (3.1) identically satisfies the continuity equation (2.1). Using equation (3.1), equation (2.6) and (2.8) become

$$(3.2)\quad \frac{\partial \Psi}{\partial y}\frac{\partial^2 \Psi}{\partial x \partial y} - \frac{\partial \Psi}{\partial x}\frac{\partial^2 \Psi}{\partial y^2} = \frac{1}{\rho}\left\{\frac{\partial}{\partial y}\left[K|\frac{\partial^2 \Psi}{\partial y^2}|^{n-1}\frac{\partial^2 \Psi}{\partial y^2}\right]\right\} - \left(\frac{1}{\bar{\rho A}} + \frac{\sigma B^2}{\rho}\right)\left(\frac{\partial \Psi}{\partial y} - U_\infty\right),$$

$$(3.3)\quad \frac{\partial \Psi}{\partial y}\frac{\partial T}{\partial x} - \frac{\partial \Psi}{\partial x}\frac{\partial T}{\partial y} = \frac{1}{\rho C_p}\left\{\frac{\partial}{\partial y}\left[\kappa_\infty\left(1 + \epsilon\frac{T - T_\infty}{\Delta T}\right)\frac{\partial T}{\partial y}\right] + \frac{16 T_\infty^3 \sigma}{3\kappa}\frac{\partial^2 T}{\partial y^2}\right\} + \frac{\sigma B^2}{\rho C_p}\left(\frac{\partial \Psi}{\partial y}\right)^2 + \frac{Q}{\rho C_p}(T - T_\infty).$$

The boundary conditions are transformed into

$$(3.4)\quad \begin{cases} \frac{\partial \Psi}{\partial y} = L_1 \frac{\partial^2 \Psi}{\partial y^2}, \frac{\partial \Psi}{\partial x} = -v_w, T = T_w + D_1 \frac{\partial T}{\partial y} \text{ at } y = 0, \\ \frac{\partial \Psi}{\partial y} \to U_\infty, T \to T_\infty \text{ as } y \to \infty, \end{cases}$$

where

$$L_1 = L\frac{U_\infty \rho}{K}\left(\frac{Kx}{\rho U_\infty^{2-n}}\right)^{\frac{1}{n+1}}$$

is the velocity slip factor and

$$D_1 = D\frac{U_\infty \rho}{K}\left(\frac{Kx}{\rho U_\infty^{2-n}}\right)^{\frac{1}{n+1}}$$

is the thermal slip factor. Here L and D are the initial values of velocity and thermal slip parameters, respectively.

We introduce the following dimensionless similarity variable (η), dimensionless stream function $\Psi(\eta)$ and dimensionless temperature $\theta(\eta)$ of the form

$$(3.5)\quad \eta = \left(\frac{Re}{\frac{x}{L}}\right)^{\frac{1}{n+1}}\frac{y}{L}, \Psi(x, y) = LU_\infty\left(\frac{\frac{x}{L}}{Re}\right)^{\frac{1}{n+1}} f(\eta), \theta(\eta) = \frac{T - T_\infty}{\Delta T},$$

where $Re = \frac{\rho U_\infty^{2-n} L^n}{K}$ is the generalized Reynolds number. Using equation (3.5) into equation (3.2) and (3.3), we obtain the following system of ODE

$$(3.6)\quad n|f''|^{n-1} f''' + \frac{1}{n+1} f f'' - (k + M)(f' - 1) = 0,$$

$$(3.7)\quad \theta'' + \frac{Pr_\infty}{(n+1)(1 + \epsilon\theta + Nr)} f\theta' + \frac{\epsilon}{(1 + \epsilon\theta + Nr)}\theta'^2 + \frac{M Pr_\infty Ec}{(1 + \epsilon\theta + Nr)} f'^2 + \frac{Pr_\infty Q}{(1 + \epsilon\theta + Nr)}\theta = 0.$$

The corresponding boundary conditions are

$$(3.8)\quad \begin{cases} f(\eta) = S, f'(\eta) = \delta f''(\eta), \theta(\eta) = 1 + \beta\theta'(\eta) \text{ at } \eta = 0, \\ f'(\eta) \to 1, \theta(\eta) \to 0, \text{ as } \eta \to \infty, \end{cases}$$

where k is the permeability parameter, M is the magnetic parameter, Pr_∞ is the local Prandtl number, Nr is the thermal radiation parameter, S is the suction/blowing parameter, which corresponds to suction when $S > 0$, and corresponds to blowing when $S < 0$, Ec is Eckert number, Q is heat source parameter. In boundary conditions δ and β are the dimensionless velocity and thermal slip parameters, respectively. These parameters are further defined as

$$(3.9)\quad k = \frac{\mu x}{U_\infty \rho A}, M = \frac{x\sigma B^2}{U_\infty \rho}, S = -v_w \frac{x(n+1)}{U_\infty}\left(\frac{\rho U_\infty^{2-n}}{K}\right)^{\frac{1}{n+1}}, \delta = L\frac{U_\infty \rho}{K}, \beta = D\frac{U_\infty \rho}{K},$$

$$Pr_\infty = \frac{C_p}{\kappa_\infty} K^{\frac{2}{n+1}}\left(\frac{U_\infty^3 \rho}{x}\right)^{\frac{n-1}{n+1}} = (1 + \epsilon\theta) Pr, Ec = \frac{U_\infty^2}{C_{p\Delta T}},$$

where $Pr = \frac{C_p}{\kappa} K^{\frac{2}{n+1}}\left(\frac{U_\infty^3 \rho}{x}\right)^{\frac{n-1}{n+1}}$ is the Prandtl number.

4 Relevant physical measures

The shear stress is given by

$$(4.1)\quad \tau_{xy} = [K|\frac{\partial u}{\partial y}|^{n-1}\frac{\partial u}{\partial y}]_{y=0} = \rho U_\infty^2 Re_x^{-\frac{1}{(n+1)}}|f''(0)|^{n-1}f''(0).$$

The skin-friction coefficient is defined as

$$(4.2)\quad C_f = \frac{\tau_{xy}}{\rho u_\infty^2/2} = 2Re_x^{-\frac{1}{(n+1)}}|f''(0)|^{n-1}f''(0).$$

The local Nusselt number is given by
$Nu_x = -\frac{q(x)x}{\kappa(T-T_\infty)}$,
where $q(x) = -\kappa(\frac{\partial T}{\partial y})_{y=0}$is the heat flux at the surface.

$$(4.3)\quad Nu_x = -\frac{\lambda}{T_w - T_\infty}(\frac{\partial T}{\partial y})_{y=0} = -Re_x^{\frac{1}{(n+1)}}\theta'(0),$$

where λ is characteristic length.

The nonlinear coupled boundary-layer equations (3.6) and (3.7) together with the boundary conditions (3.8) are solved numerically using Runge-kutta method along with shooting technique. At first, higher-order nonlinear differential equations (3.6) and (3.7) are converted into the simultaneous nonlinear differential equations of first order and they are further transformed into initial value problem by applying the shooting technique.

Let $f = f_1, f' = f_2, f'' = f_3, \theta = f_4$, $\theta' = f_5$ then we get following system of first order differential equations:
$f_1' = f_2,$
$f_2' = f_3,$

$$(4.4)\quad f_3' = \frac{(K+M)}{n}\frac{(f_2-1)}{f_3^{(n-1)}} - \frac{f_1 f_3^{(2-n)}}{n(n+1)}, f_4' = f_5,$$

$$(4.5)\quad -f_5' = \frac{Pr}{(n+1)}\frac{(1+\epsilon f_4)}{(1+\epsilon f_4+Nr)}f_1 f_5 + \frac{\epsilon}{(1+\epsilon f_4+Nr)}f_5^2 + \frac{MPrEc(1+\epsilon f_4)}{(1+\epsilon f_4+Nr)}f_2^2 + \frac{PrQ(1+\epsilon f_4)}{(1+\epsilon f_4+Nr)}f_4$$

subject to the following boundary conditions

$$(4.6)\quad \begin{cases} f_1 = S, f_2 = \delta f_3\ f_4 = 1+\beta f_5 \text{ at } \eta = 0, \\ f_2 = 1, f_4 = 0 \text{ at } \eta = \infty, \end{cases}$$

Now, to convert above system into initial value problems, we take initial guesses of f_3 and f_5 at $\eta = 0$. The resultant initial value problems are solved by employing Runge-kutta fourth order method. The step size $\Delta\eta = 0.016$ is used to obtain the numerical solution with five decimal place accuracy as the criterion of convergence.

5 Results and discussion

Now, we shall analyse the results obtained through numerical computation for variables like power law index (n), velocity slip parameter (δ), magnetic parameter *(M)*, permeability parameter (k), suction/injection (S), thermal radiation *(Nr)*, variable thermal conductivity (ϵ), thermal slip parameter (β), Prandtl number (Pr), Eckert number (Ec) and heat source parameter (Q). The default values of the parameters are set as $M = 0.2$, $S = 0.3$, $Nr = 0.3$, $Pr = 1.2$, $Ec = 0.01$, $k = 0.3$, $\delta = 0.4, \beta = 0.4$, unless otherwise specified. Their results are presented through graphs.

***Figure*.5.1** shows the effect of velocity slip parameter on the velocity profile of shear thinning and shear thickening fluids. The comparison of curves with same power-law index shows that velocity slip at boundary and the fluid velocity within the boundary are proportionally related due to positive value of the fluid viscosity adjacent to the surface. Moreover, increase in slip parameter leads to increased flow through the boundary layer. ***Figure* 5.2(a)** and ***Figure* 5.2(b)** elucidate the effect of slip parameter on the temperature profile for $n = 0.8$ and $n = 1.3$, respectively.

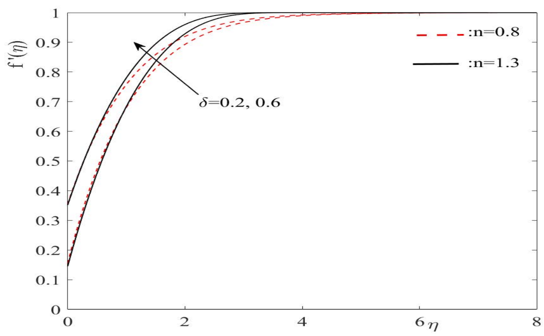

***Figure* 5.1:** Velocity profiles for different values of velocity slip parameter.

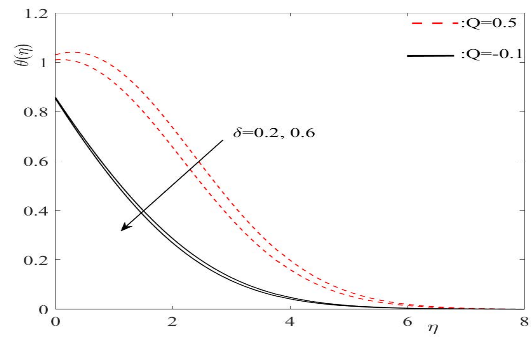

***Figure* 5.2(a):** Velocity profiles for different values of velocity slip parameter.

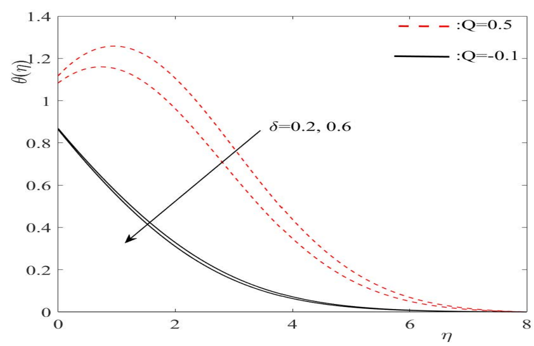

***Figure* 5.2(b):** Temperature profiles for different values of velocity slip parameter for n = 1.3.

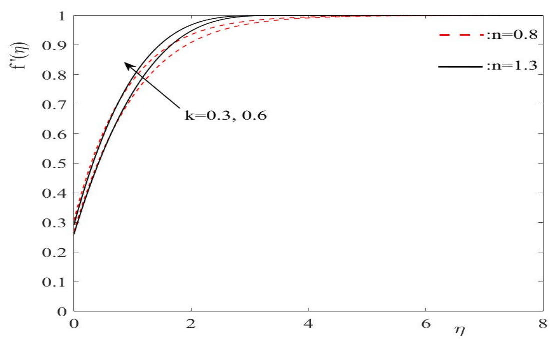

***Figure* 5.3:** Velocity profiles for different values of permeability parameter.

It is evident from ***Figure* 5.2(a)** and ***Figure* 5.2(b)** that an increase in the velocity slip parameter leads to a decrease in the temperature profile. The effect of permeability parameter on fluid velocity profile is shown in ***Figure* 5.3.** It is noticed that an increase in porosity, the magnitude of Darcian body force reduces, which increases the velocity of the fluid in the boundary layer. It is clear from the ***Figure* 5.3**. that initially, shear-thinning fluid increases faster than shear-thickening fluid. This is due to the smallest effective viscosity of shear-thinning fluids. While the opposite trend is seen in later time as the viscosity of the shear thickening fluid will reduce.

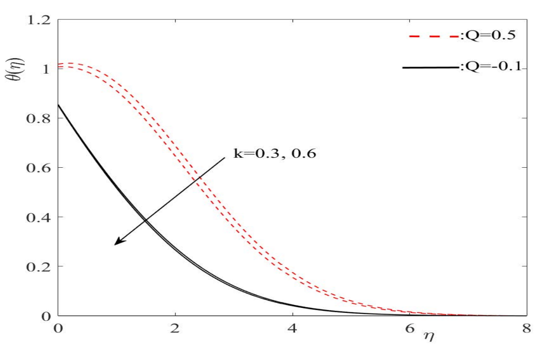

***Figure* 5.4(a):** Temperature profiles for different values of permeability parameter for n= 0.8.

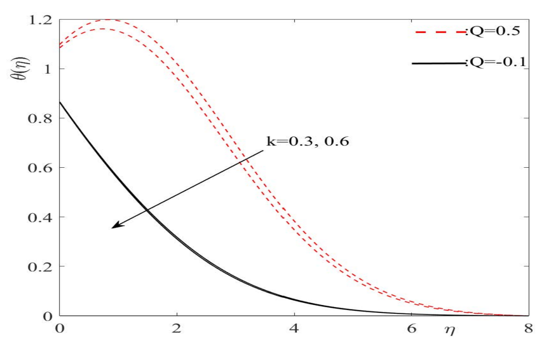

***Figure* 5.4(b):** Temperature profiles for different values of permeability parameter for n = 1.3.

***Figure* 5.4(a)** and ***Figure* 5.4(b)** elucidate the effect of permeability parameter on the temperature profile for $n = 0.8$ and $n = 1.3$, respectively. It is observed that the increase in permeability parameter leads to an increase in the heat transfer rate and a decrease in the thickness of the thermal boundary layer. ***Figure* 5.5** exhibits the effect of magnetic parameter on the velocity profile. It is clear from the figure that the increase in magnetic field causes an increase in the velocity profile. ***Figure* 5.6(a)** and ***Figure* 5.6(b)** display the influence of magnetic parameter on the temperature profile for $n = 0.8$ and $n = 1.3$, respectively. In the case of heat source, the temperature profile decreases with increasing value of magnetic parameter.

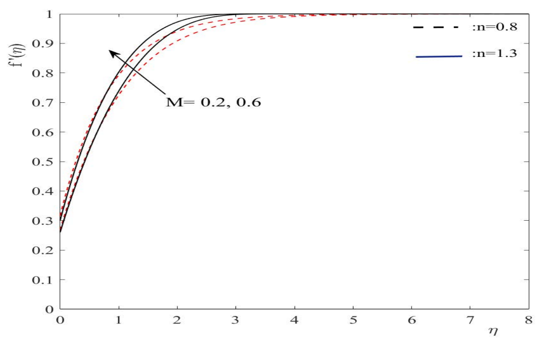

***Figure* 5.5:** Velocity profiles for different values of Magnetic parameter.

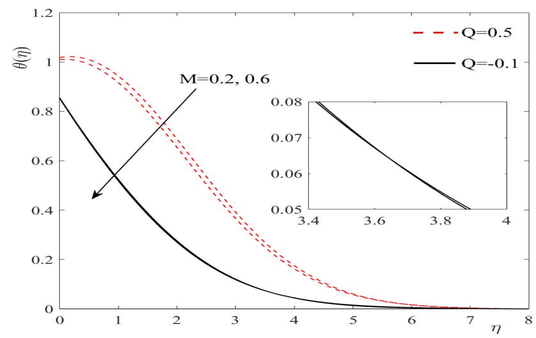

***Figure* 5.6(a):** Temperature profiles for different values of Magnetic parameter for n= 0.8.

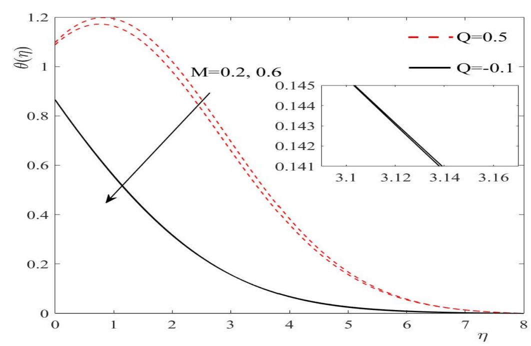

***Figure* 5.6(b):** Temperature profiles for different values of Magnetic parameter for n = 1.3.

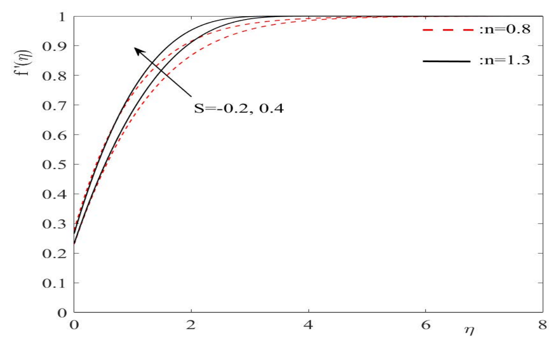

***Figure* 5.7:** Velocity profiles for different values of suction/injection parameter.

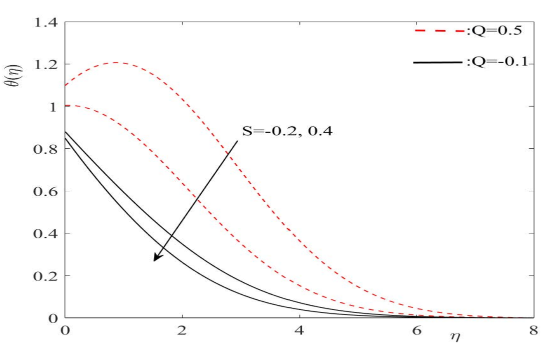

***Figure* 5.8(a):** Temperature profiles for different values of suction/injection parameter for n = 0.8.

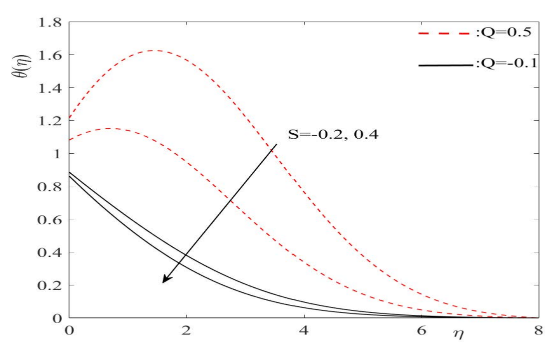

***Figure* 5.8(b):** Temperature profiles for different values of suction/injection parameter for n = 1.3.

It is clear from ***Figure* 5.6(a)** that in the case of the heat sink, initially, temperature profile decreases with increasing value of magnetic parameter but far from the plate for $\eta > 3.6$, the temperature profile increase with increasing value of the magnetic parameter. The same effect in the temperature profile is seen in ***Figure* 5.6(b)** for $\eta > 3.12$. ***Figure***

5.7 presents the effect of the suction/injection parameter on the velocity profile for porous sheet in the presence of slip conditions and magnetic fields in a porous medium. It is evident from the ***Figure* 5.7**, that velocity profile increases with the increasing value of suction/injection parameter. ***Figure* 5.8(a)** and ***Figure* 5.8(b)** are drawn to discuss the effect of suction/injection parameter on the temperature profile for $n = 0.8$ and $n = 1.3$, respectively. From ***Figure* 5.8(a)** and ***Figure* 5.8(b)**, it is seen that temperature profile decreases as the value of S increases which results in the increased rate of heat transfer through the boundary layer. ***Figure* 5.9(a)** and ***Figure* 5.9(b)** describe the impact of Prandtl number on the temperature profile for $n = 0.8$ and $n = 1.3$, respectively. The thermal conductivity of the fluid declines by enhancing the Prandtl number. Thus transfer of the heat slows which fall down the temperature of flow distribution. ***Figure* 5.9(a)** and ***Figure* 5.9(b)** validates the above results i.e. the temperature of the flow distribution falls when Prandtl number increases. In the case of heat source, near the plate temperature profile increases due to slip effect and far from the plate the temperature profile decreases with increasing value of Prandtl number. In the case of the heat sink, the temperature profile decreases with the increasing value of the Prandtl number.

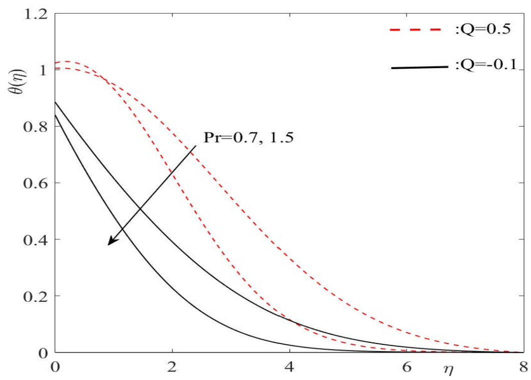

***Figure* 5.9(a):** Temperature profiles for different values of Prandtl number for $n = 0.8$.

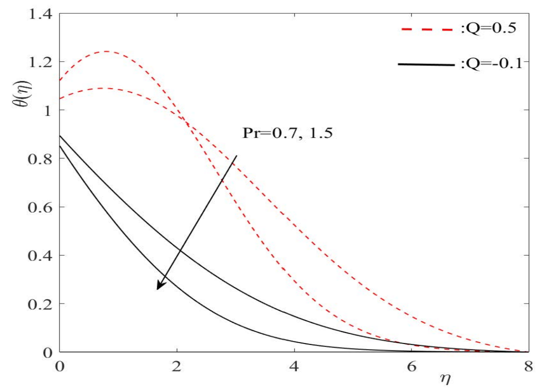

***Figure* 5.9(b):** Temperature profiles for different values of Prandtl number for $n = 1.3$.

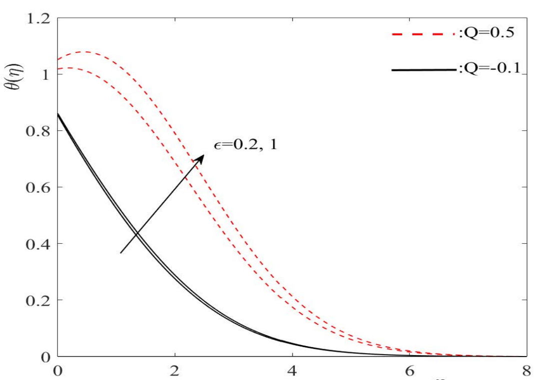

***Figure* 5.10(a):** Temperature profiles for different values of thermal conductivity parameter for $n = 0.8$.

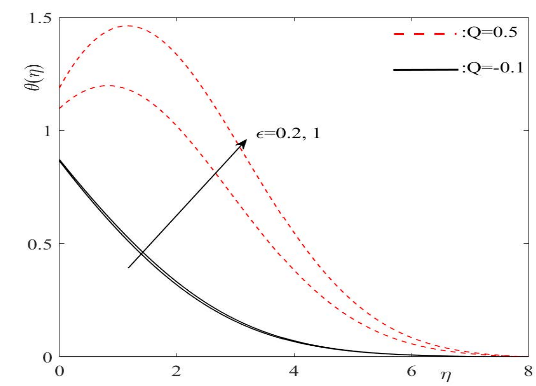

***Figure* 5.10(b):** Temperature profiles for different values of thermal conductivity parameter for $n = 1.3$.

***Figure* 5.10(a)** and ***Figure* 5.10(b)** depict the effect of the thermal conductivity parameter on the temperature profile for $n = 0.8$ and $n = 1.3$, respectively. The results show that with the increase in the thermal conductivity parameter, the temperature profile increases ***Figure* 5.11(a)** and ***Figure* 5.11(b)** reveals the usual effect of the thermal slip parameter on the temperature profile for $n = 0.8$ and $n = 1.3$, respectively. It is evident from the **Fig.5.11(a)** and ***Figure* 5.11(b)** that in the case of $Q > 0$, the temperature increases with increasing values of thermal slip parameter. The reverse happens in the case of the $Q < 0$. ***Figure* 5.12(a)** and ***Figure* 5.12(b)** show the effect of the thermal radiation parameter on the temperature profile for $n = 0.8$ and $n = 1.3$, respectively.

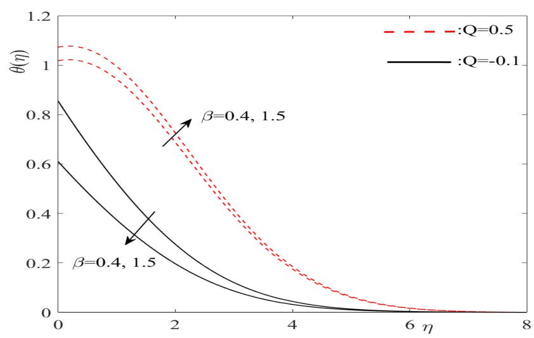

***Figure* 5.11(a):** Temperature profiles for different values of thermal slip parameter for n = 0.8.

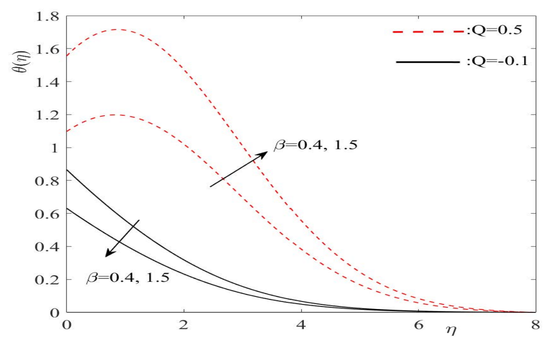

***Figure* 5.11(b):** Temperature profiles for different values of thermal slip parameter for n = 1.3.

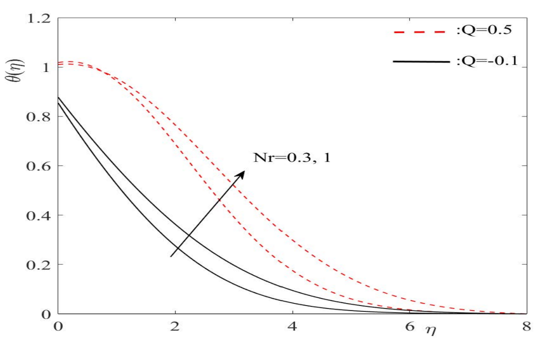

***Figure* 5.12(a):** Temperature profiles for different values of thermal radiation parameter for n = 0.8.

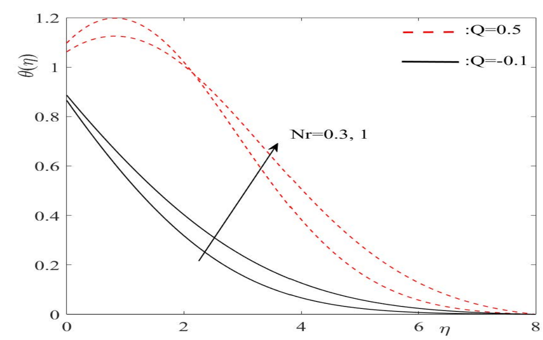

***Figure* 5.12(b):** Temperature profiles for different values of thermal radiation parameter for n = 1.3.

It is depicted from the ***Figure* 5.12(a)** and ***Figure* 5.12(b)** that in the case of heat source, near the plate temperature profile decrease with increasing value of thermal radiation parameter and far from the plate the temperature profile increases with increasing value of thermal radiation parameter. In the case of the heat sink, the temperature profile increases with the increasing value of the thermal radiation parameter.

***Figure* 5.13(a)** and ***Figure* 5.13(b)** demonstrate the temperature distribution for the different values of Eckert number for n = 0.8 and n = 1.3, respectively. Eckert number expresses the relationship between flow kinetic energy to the boundry layer enthalpy difference. So an increase in Eckert number causes an enlargement in kinetic energy, hence temprature of the fluid rises. It is observed from ***Figure* 5.13(a)** and ***Figure* 5.13(b)** that temperature profile increases with the increasing values of Eckert number.

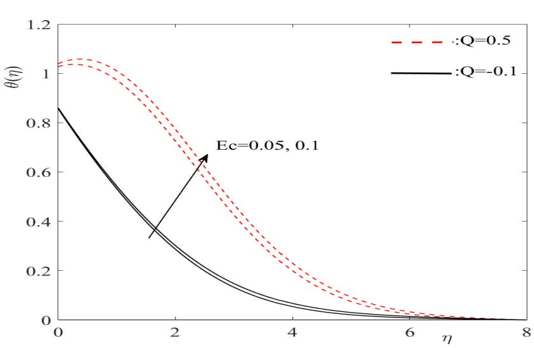

***Figure* 5.13(a):** TTemperature profiles for different values of Eckert number for n = 0.8.

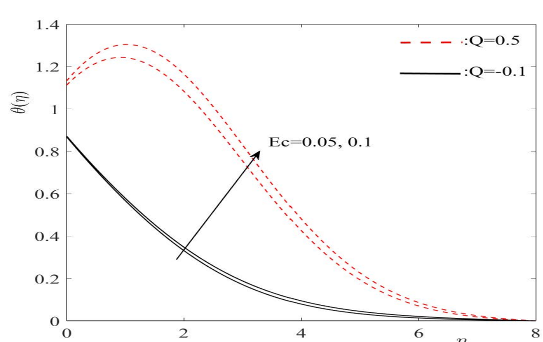

***Figure* 5.13(b):** Temperature profiles for different values of Eckert number for n = 1.3.

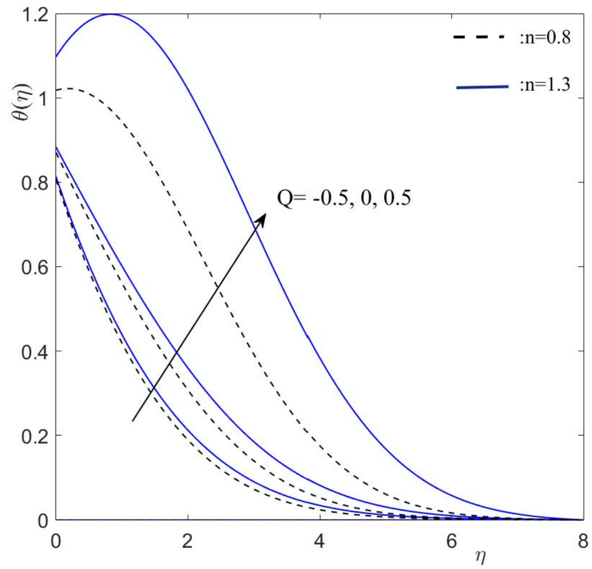

***Figure* 5.14:** Temperature profiles for different values of heat source/sink parameter.

***Figure* 5.14** depicts the effect of heat source/sink parameter on temperature profile. It is observed that the temperature profile increases with the increasing values of heat source/sink parameter.

***Table* 5.1** shows the nature of the skin friction coefficient for various physical parameters. It is observed that the shear-thinning fluid has greater values of skin friction coefficient as compared to shear thickening fluid. The skin friction coefficient increases with an increase in magnetic parameter, permeability parameter and suction/injection parameter and the skin friction coefficient decreasing with an increase in slip parameter.

***Table* 5.1:** Comparison of $f''(0)$ for the different values of parameters k, M, δ and S for n= 0.8 (Shear thinning) and n=1.3 (Shear thickening).

n	k	M	S	δ	$f''(0)$
0.8	0.3	0.2	0.3	0.4	0.672091
1.3					0.650778
0.8	0.6	0.2	0.3	0.4	0.76586
1.3					0.729205
0.8	0.3	0.6	0.3	0.4	0.79212
1.3					0.751132
0.8	0.3	0.2	0.3	0.6	0.59158
1.3					0.586712
0.8	0.3	0.2	-0.2	0.4	0.575742
			0.4		0.691872
1.3			-0.2		0.580588
			0.4		0.66491

***Table* 5.2** shows the values of Nusselt number for different physical parameters concerning power law index 0.8 and 1.3 respectively. It is observed that the Nusselt number decreases with an increase in power law index. It is noticed from the table that the Nusselt number increases with an increase in suction/injection parameter, permeability parameter, magnetic parameter and slip parameter while the reverse effect is seen in the case of thermal slip parameter, Eckert number, thermal conductivity parameter and heat source/sink parameter. In the case of the heat source, the Nusselt number decreases with the increasing values of the Prandtl number. In the case of the heat sink, the Nusselt number increases with the increasing values of the Prandtl number: in the case of heat source, the Nusselt number increases with the increasing values of the thermal radiation parameter while Nusselt number decreases with the increasing values of the thermal radiation parameter in the case of heat sink.

Table **5.2:** Comparison of $-\theta'(0)$ for the different values of parameters k, M, δ, S, β, Pr, Nr, Ec, Q and ϵ for $n = 0.8$ (Shear thinning) and $n = 1.3$ (Shear thickening).

S	k	M	δ	β	Pr	Nr	Ec	ε	Q	$-\theta'(0)$ **for n= 0.8**	$-\theta'(0)$ **for n= 1.3**
-0.2	0.3	0.2	0.4	0.4	1.2	0.3	0.01	0.2	0.5	-0.24471	-0.53755
									-0.1	0.299094	0.286279
0.4									0.5	-0.01121	-0.2007
									-0.1	0.376295	0.34617
0.3	0.6	0.2	0.4	0.4	1.2	0.3	0.01	0.2	0.5	-0.01863	-0.20963
									-0.1	0.369373	0.340504
0.3	0.3	0.2	0.4	0.4	1.2	0.3	0.01	0.2	0.5	-0.044945	-0.24344
									-0.1	0.36323	0.336027
		0.6							0.5	-0.02397	-0.21995
									-0.1	0.367622	0.338097
0.3	0.3	0.2	0.2	0.4	1.2	0.3	0.01	0.2	0.5	-0.07463	-0.29373
									-0.1	0.355587	0.329055
			0.6						0.5	-0.02416	-0.2089
									-0.1	0.368908	0.34139
0.3	0.3	0.2	0.4	0.4	1.2	0.3	0.01	0.2	0.5	-0.044928	-0.24344
									-0.1	0.363236	0.336027
				1.5					0.5	-0.048414	-0.37053
									-0.1	0.260026	0.245742
0.3	0.3	0.2	0.4	0.4	0.7	0.3	0.01	0.2	0.5	-0.012404	-0.11564
									-0.1	0.28659	0.265737
					1.5				0.5	-0.058841	-0.30329
									-0.1	0.400579	0.370406
0.3	0.3	0.2	0.4	0.4	1.2	1	0.01	0.2	0.5	-0.02521	-0.15452
									-0.1	0.305735	0.283336
0.3	0.3	0.2	0.4	0.4	1.2	0.3	0.05	0.2	0.5	-0.0688	-0.282
									-0.1	0.35695	0.32923
							0.1		0.5	-0.099	-0.3318
									-0.1	0.34911	0.32075
0.3	0.3	0.2	0.4	0.4	1.2	0.3	0.01	1	0.5	-0.12761	-0.47219
									-0.1	0.347678	0.321791
0.3	0.3	0.2	0.4	0.4	1.2	0.3	0.01	0.2	0.5	-0.045	-0.2435
									0	0.32373	0.2915
									-0.5	0.4833	0.46618

6 Conclusions

In this paper, we have discussed the MHD flow and heat transfer of a non-Newtonian power-law fluid over a porous sheet in the presence of heat source/sink, joule heating and partial slip conditions. The magnetic parameter, Prandtl number, Eckert number, heat source/sink parameter are varied in the ranges 0.2 to 0.6, 0.7 to 1.5, 0.05 to 0.1, and -0.5 to 0.5, respectively. According to the study the following conclusions are made:

1. The increase in magnetic field causes to increase in the velocity profile and decrease in the temperature profile.
2. The temperature profile decreases with increasing values of the Prandtl number under slip condition.
3. The temperature profile increases with increasing values of Eckert number under slip condition.
4. The temperature profile increases with increasing values of heat source/sink parameter under slip condition.
5. The skin friction coefficient increases with an increase in section/injection.
6. The Nusselt number increses with an increase in sectiom/injection parameter, permeability parameter or thermal radiation parameter when $Q > 0$.

Acknowledgement. The authors thank to the Editor and reviewers for their constructive remarks and useful suggestions.

References

[1] G. M. Abdel-Rahman, Effect of variable viscosity and thermal conductivity on unsteady *MHD* flow of non-Newtonian fluid over a stretching porous sheet, Thermal Science, **17** (2013), 1035-1047.

[2] M. S. Abel, P. S. Datti and N. Mahesha, Flow and heat transfer in a power-law fluid over a stretching sheet with variable thermal conductivity and non-uniform heat source, *International Journal of Heat and Mass Transfer*, **52** (2009), 2902-2913.

[3] H. I. Andersson and T.H. Toften, Numerical solution of the laminar boundary layer equation for power-law fluids, *Journal of Non-Newtonian Fluid Mechanics*, **32** (1989), 175-195.

[4] H. I. Andersson and E.de. Korte, MHD flow of a power-law fluid over a rotating disk, *European Journal of Mechanics B/Fluids*, **21** (2002), 317-324.

[5] H. I. Andersson, Trondheim and Norway, Slip flow past a stretching surface, *Acta Mechanica*, **158** (2002), 121-125.

[6] A. Aziz, Y. All, T. Aziz and J.L. Siddique, Heat transfer analysis for stationary boundary layer slip flow of a power-law fluid in a Darcy porous medium with plate suction/Injection, *PLOS ONE*, **10** (2015), e0138855(1-13).

[7] A. Aziz, T. Aziz and J.L. Siddique, Steady boundary layer slip flow along with heat and mass transfer over a flat porous plate embedded in a porous medium, *PLOS ONE*, **9** (2014), e114544(1-14).

[8] Alberta, Edmonton, J. P. Pascal and H. Pascal, ON some similarity solutions to shear flows of non-Newtonian power-law fluids, *Acta Mechanica*, **112** (1995), 229-236.

[9] R. Bird, W. Stewart and E. Lightfoot, Transport Phenomena, John Wiley and Sons, New York, USA, 1960.

[10] C. H. Chen, Effect of magnetic field and suction/injection on convection heat transfer of non-Newtonian power-law fluids past a power-law stretched sheet with surface heat flux, *International Journal of Thermal Sciences*, **47** (2008), 954-961.

[11] R. Chhabra and J. F. Richardson, *Non-Newtonian Flow and Applied Rheology: Engineering Applications*, Butterworth-Heinemnn, Oxford, UK, 2^{nd}, 2008.

[12] K. Das, Slip effect on heat and mass transfer in MHD micropolar fluid over an inclined plate with thermal radiation and chemical reaction, *International Journal for Numerical Methods in Fluids*, **70** (2012), 96-113.

[13] P. S. Gupta and A. S. Gupta, Heat and mass transfer on a stretching sheet with suction or blowing, *The Canadian Journal of Chemical Engineering*, **55** (1977), 744-746.

[14] M. Kiyasatfar and N. Pourmahmoud, Laminar MHD flow and heat transfer of power-law fluids in square microchannels, *International Journal of Thermal Sciences*, **99** (2016), 26-35.

[15] A. A. M. Mahmoud, Slip velocity effect on a non -Newtonian power-law fluid over a moving permeable surface with heat generation, *Mathematical and Computer Modelling*, **54** (2011), 1228-1237.

[16] O. D. Makinde, Free convection flow with thermal radiation and mass transfer past a moving vertical porous plate, *International Communications in Heat and Mass Transfer*, **32** (2005), 1411-1419.

[17] S. Mukhopadhyay, Heat transfer analysis of the unsteady flow of a Maxwell fluid over a stretching surface in the presence of a heat source/sink, *Chinese Physics Letters*, **29** (2012), 054703(1-4).

[18] P. R. Sharma and P. Mathur, Steady laminar free convection flow of an electrically conducting fluid along a porous hot vertical plate in the presence of heat source/sink, *Indian Journal Pure Applied Mathematics*, **26** (1995), 1125-1134.

[19] T. Sarpkaya, Flow of non-Newtonian fluids in a magnetic field, *AIChE Journal*, **7** (1961), 324-328.

[20] J. D. Savins, Non-Newtonian flow through porous media, *Industrial and Engineering Chemistry*, **61** (1969), 18-47.

[21] W. R. Schowalter, The application of Boundary-layer theory to power-law pseudoplastic fluids: similar solutions, *AIChE Journal*, **6** (1960), 24-28.

[22] M. Yurusoy, Unsteady boundary layer flow of power-law fluid on stretching sheet surface, *International Journal of Engineering Science*, **44** (2006), 325-332.